Supplementary Material (ESI) for Dalton Transactions

Supporting Information

Role of the orientation of –OH groups on sensitivity and selectivity of the interaction of M^{2+} with ribosyl- and galctosyl-imino-conjugates: Solution recognition studies of M^{2+} in MeOH and selective recognition of Cu^{2+} in HEPES buffer, and first crystal structure determination of dinuclear-Cu(II) complexes based on both the glyco-imino-conjugates

Nitin K. Singhal,[a] Atanu Mitra,[a] G. Rajsekhar,[a] Mobin M. Shaikh,[a] Subodh Kumar,[a] Philippe Guionneau[b] and Chebrolu P. Rao[a,*]

[a]Bioinorganic Laboratory, Department of Chemistry, Indian Institute of Technology Bombay, Powai, Mumbai – 400 076, India. E-mail: cprao@iitb.ac.in

[b]Institut de Chimie la Matiere Condensee de Bordeaux, UPR 9048 CNRS 87 Av. Dr. A Schweitzer, 33608 Pessac Cedex, France

SI 01 Synthesis and characterization of L_1, L_2 and L_3

N-(O-hydroxynaphthalen-1-yl)-β-D- ribopyranosylamine (L_1): To an ethanolic suspension of crude β-D-ribopyranosyl-C1-NH_2 (1.325g, 8.83 mmol), α-hydroxynaphthaldehyde (1.549 g, 9 mmol) was added and then reaction mixture was stirred for 12 hrs. The solid separated from clear solution was filtered and washed with cold ethanol until the washings were free from impurities.

N-(2-hydroxybenzylidine)- β- D-galactopyranosylamine (L_2) to a suspension of β-D-galactopyranosyl-C1-deoxy-C1-amine (galactosyl-C1-NH_2, 3.86 g, 20 mmol) in 45 ml ethanol, salicylaldhyde (R′-CHO, 2.2 ml, 20.96 mmol) was added and the reaction mixture was allowed to reflux for 6 hrs. During the course of reflux, yellow solid was formed. The reaction mixture was allowed to cool at room temperature and was left as such overnight. Some more solid was formed which was then separated by filtration and washed with a small portion of methanol and then with petroleum ether. The filtrate was concentrated to dryness and dichloromethane as added to dissolve the pasty mass. To that petroleum ether was added to result in a second crop of solid. Yield: 5.2g, 85%; IR (KBr): 3394(b) $\upsilon_{(O-H)}$ and $\upsilon_{(N-H)}$, 2938(S), 2935(S) and 2920(S) $\upsilon_{(C-H)}$, 1631(S) $\delta_{(CH=N)}.cm^{-1}$; ^{1}HNMR (DMSO-d_6): δ 3.250-3.780(m, 5H, C2-H, C3-H, C4-H, C5-H), 4.363-4.384(d, H, $^3J_{CH1-CH-2}$,8.239HzC1-H),4.538-5.146(d, 3H, C2-OH, C3-OH, & C4-OH), 4.660-4.687(t, H,C6-OH),6.89-7.59(m, 4H, Ar-OH), 8.34(S, H, CH=N), 13.257(S, H, Ar-H)ppm. FABMS: m/z 180 ([M+H] $^+$, 90%), 179 ([M^+], 30%). Anal. calcd. for [$C_{13}H_{17}O_6N.H_2O$]: C, 55.14; H, 6.00; N, 4.95 found C, 55.08; H, 6.12; N, 5.10.

N-(o-hydroxynaphthalen-1-yl)-β-D- galactopyranosylamine(L_3)- To a suspension of β-D- galactopyranosyl-C1-deoxy-C1-amine (galactosyl-C1-NH_2, 3.86 g, 20 mmol) in 45 ml ethanol, β-hydroxy napthaldehyde (R-CHO; 2.2 g, 20.96 mmol) was added and then the reaction mixture was allowed to reflux for 6 h. During the course of reflux, yellow solid was formed. The reaction mixture was allowed to cool at room temperature and was left as such overnight. Some more solid was formed which was then separated by filtration and washed with a small portion of methanol and then with petroleum ether. Yield, (4.01g, 70%); IR (KBr): 3320(b) $\upsilon_{(O-H)}$ and $\upsilon_{(N-H)}$, 2940(S), 2975(S) and 2910(S) $\upsilon_{(C-H)}$, 1660(S) $\delta_{(CH=N)}.cm^{-1}$; ^{1}H NMR(DMSO-d_6):3.12-3.57(m. 6H, C2-H, C3-H, C-4H, , C6-H), 3.72-3.75(m, H, C5-H), 4.36-5.38(m,4H, C2-OH, C3-OH, C-4OH, C6-OH), 4.62(d, H, $^3J_{C1-H-C2-H}$ 11.02 Hz, C1-H), 6.77-7.81(m, 6H, Ar-H), 8.11(S, H, CH=N), 14.21(S, H, Phenol-OH) ppm; ^{13}C NMR(DMSO-d_6): δ 91.10(C1), 60.68-77.76(C2-C6), 106.20-137.52(Ar-10C), 158.10(CH=N) ppm; FABMS: m/z 334 ([M+H] $^+$, 70%), 333 ([M^+], 40%) Anal. calcd. for $C_{17}H_{21}O_6N$: C, 61.24; H, 5.75; N, 4.20 found C, 61.22; H, 6.00; N, 3.94.

^{1}H NMR, FT IR and mass spectra are given in figures F 01a, F 01b and F 01c respectively for L_1, L_2 and L_3.

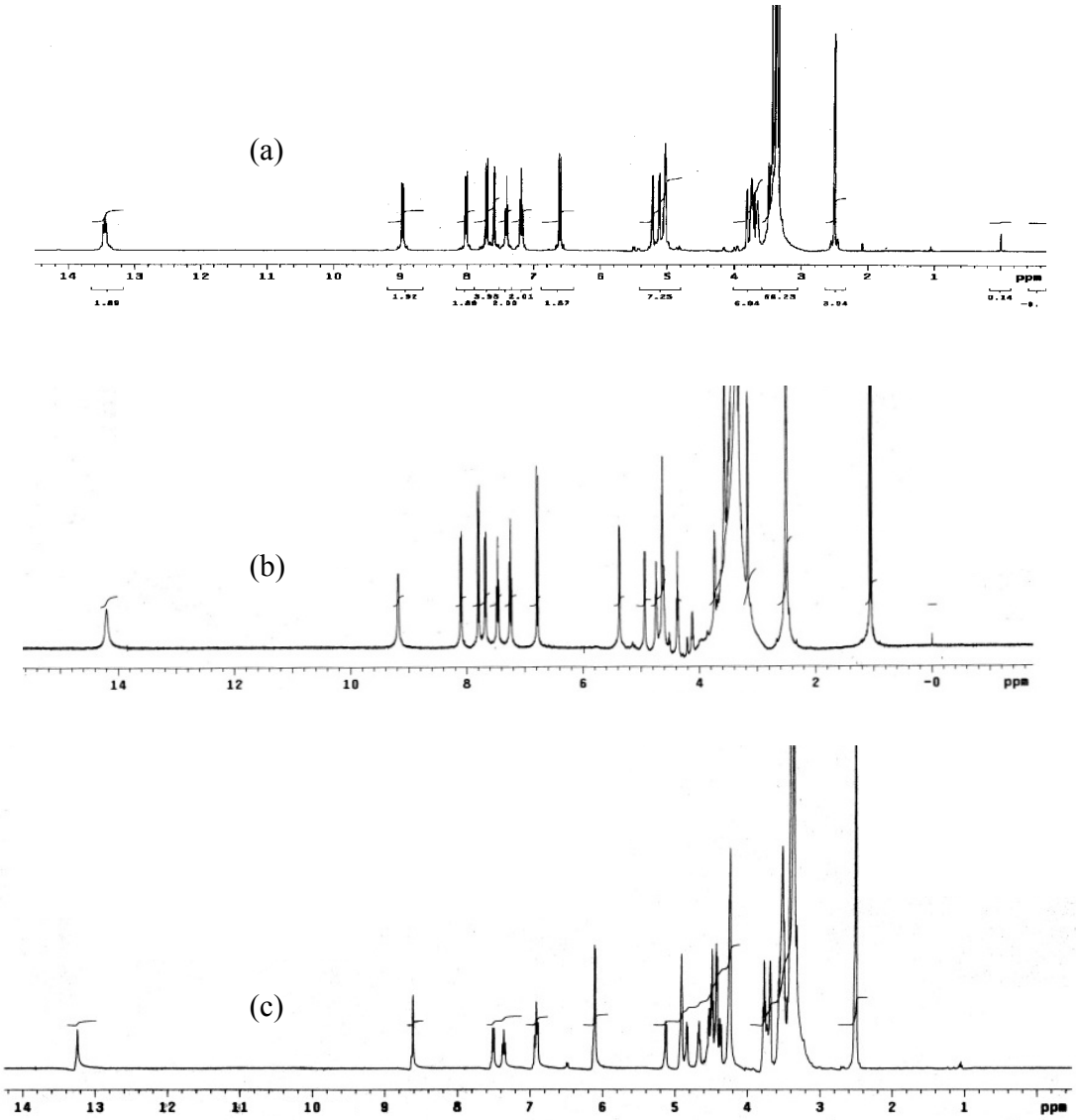

Figure F 01a. (a) ^{1}H NMR L_1, (b) L_2 and (c) L_3 in DMSO-d_6.

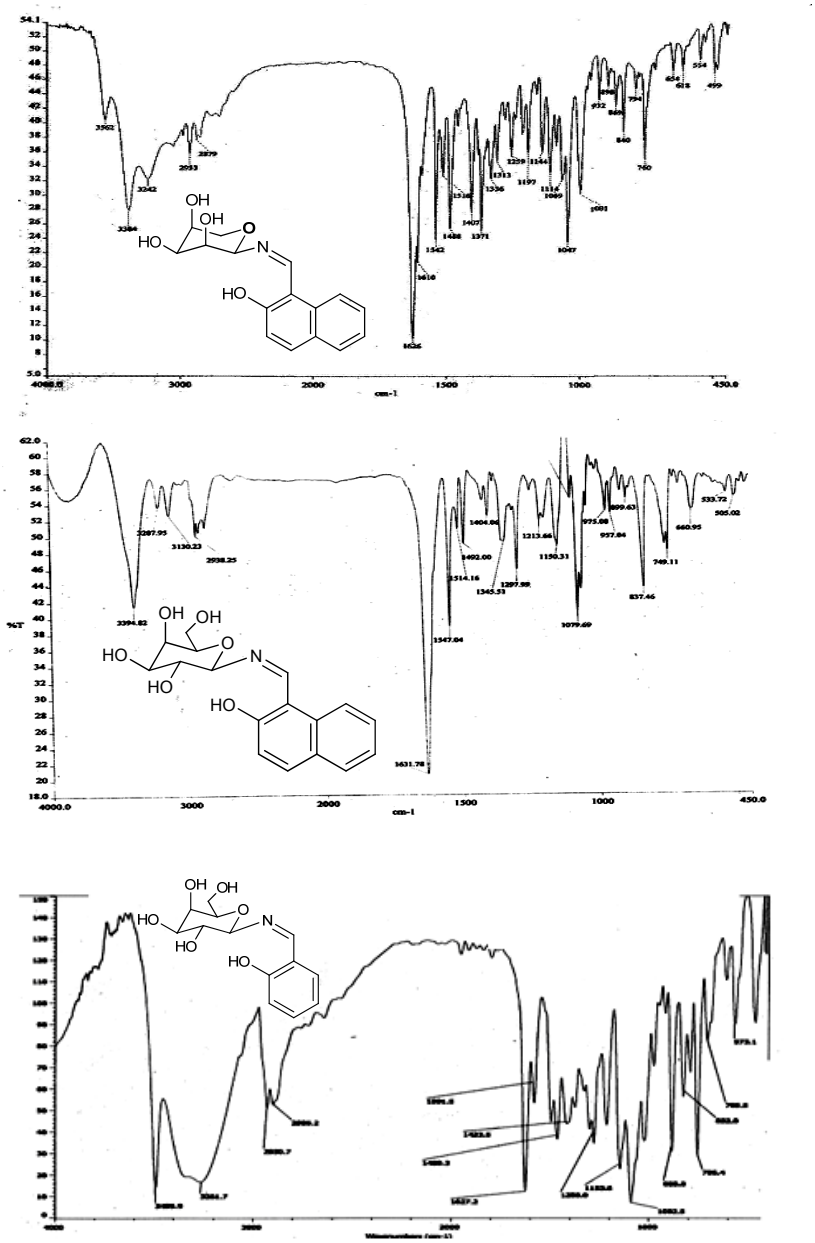

Figure F 01b. FR-IR spectra for: L_1 (top); L_2 (middle); L_3 (bottom) in KBr matrix.

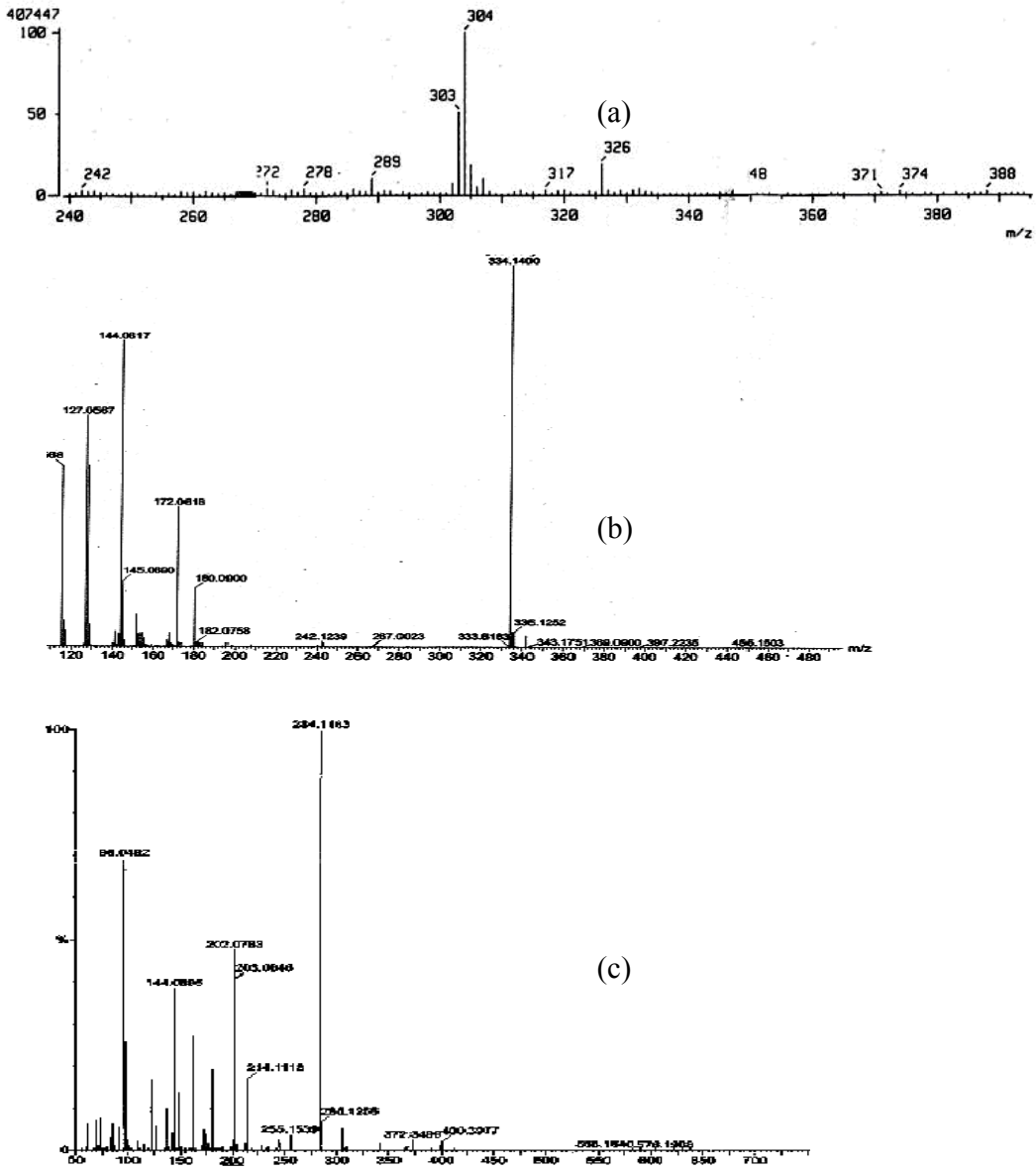

Figure F 01c. FAB mass spectra: (a) L_1, (b) L_2 and (c) L_3.

SI 02a: Absorption titration of L_1 against M^{2+} in CH_3OH

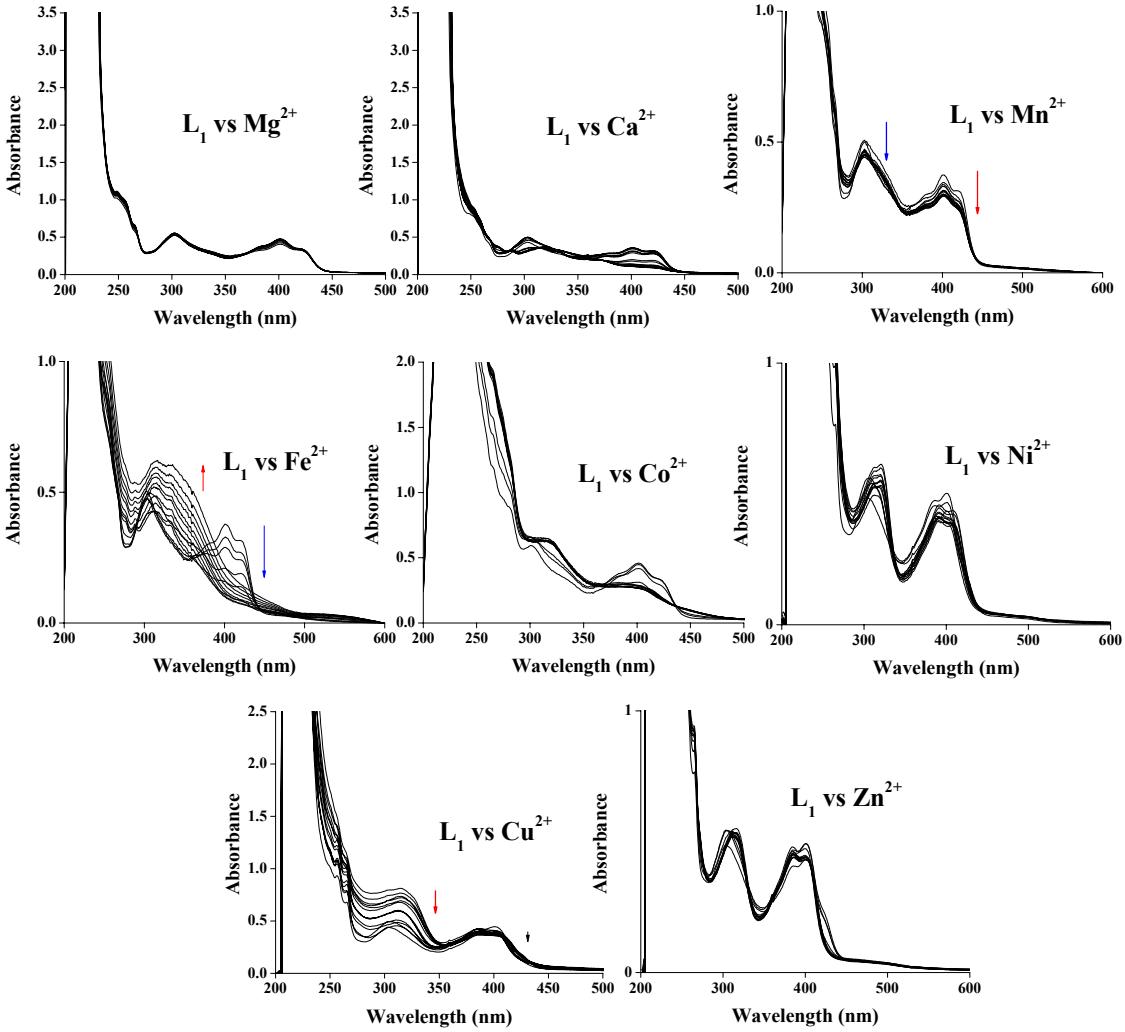

Figure F 02a. UV-Vis absorption spectra of M^{2+} titration with L_1 in MeOH.

SI 03a: Fluorescence titration for L_2 against Cu^{2+} and Zn^{2+} in CH_3OH

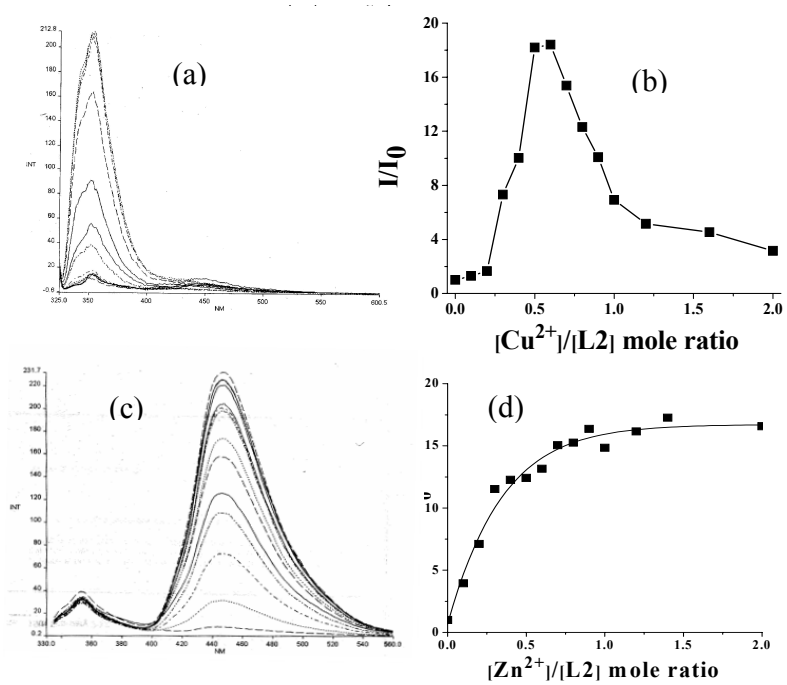

SI 03a: Fluorescence titration for L_2 against (a) & (b) vs. Cu^{2+} and (c) & (d) vs. Zn^{2+} in CH_3OH

SI 03b: Absorption titration for L_2 against M^{2+} in CH_3OH ($M=Mn^{2+}$, Fe^{2+}, Co^{2+}, Ni^{2+})

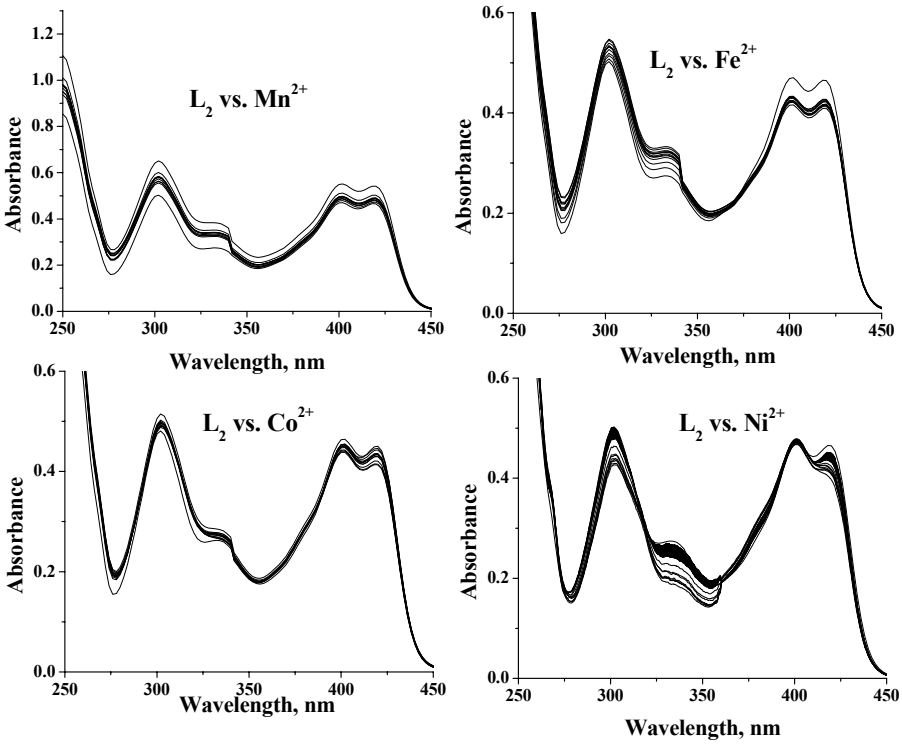

Figure F 03b. UV-Vis absorption spectra of M^{2+} titration with L_2 in MeOH.

SI 04: Absorption titration of L_3 against M^{2+} in methanol

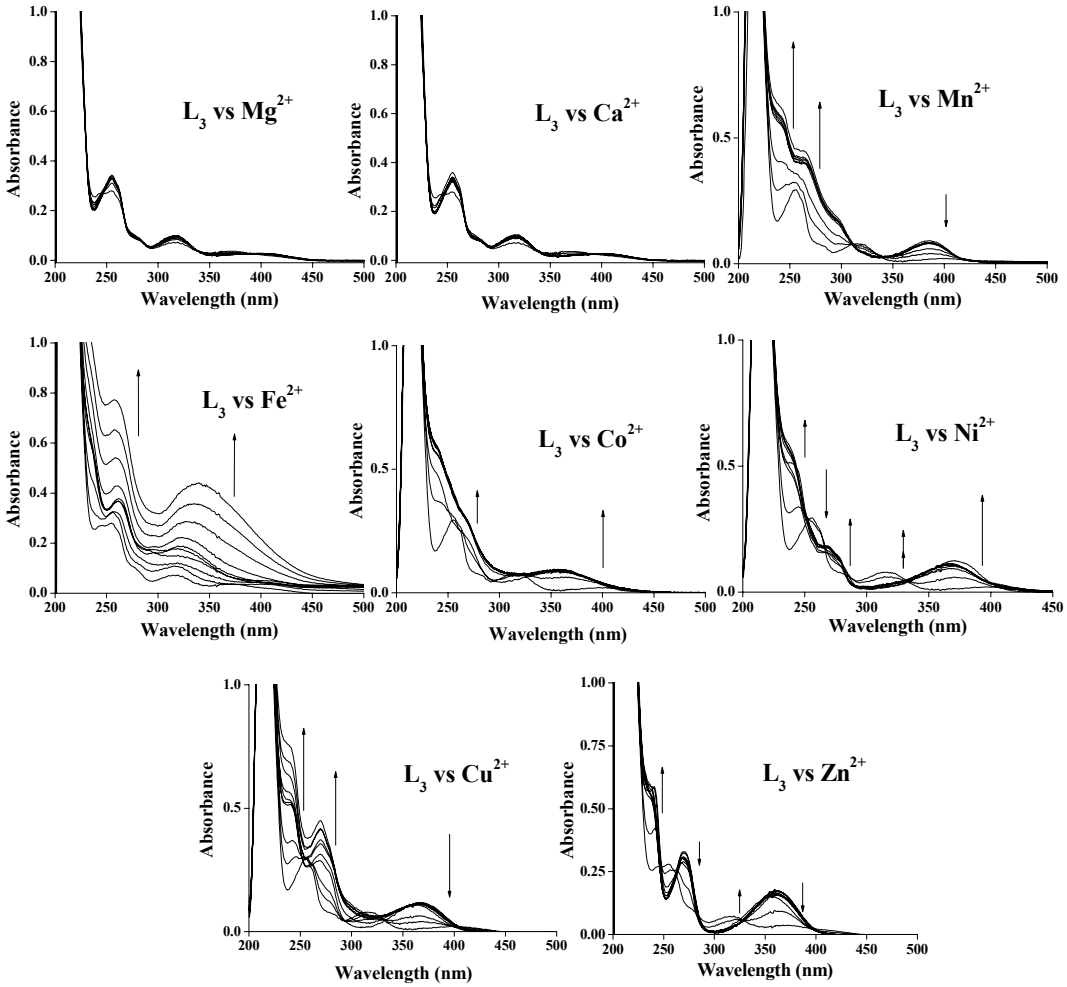

Figure F 04a. UV-Vis absorption spectra of M^{2+} titration with L_3 in MeOH.

SI 05: Competitive metal ion titration for L_1 in methanol.

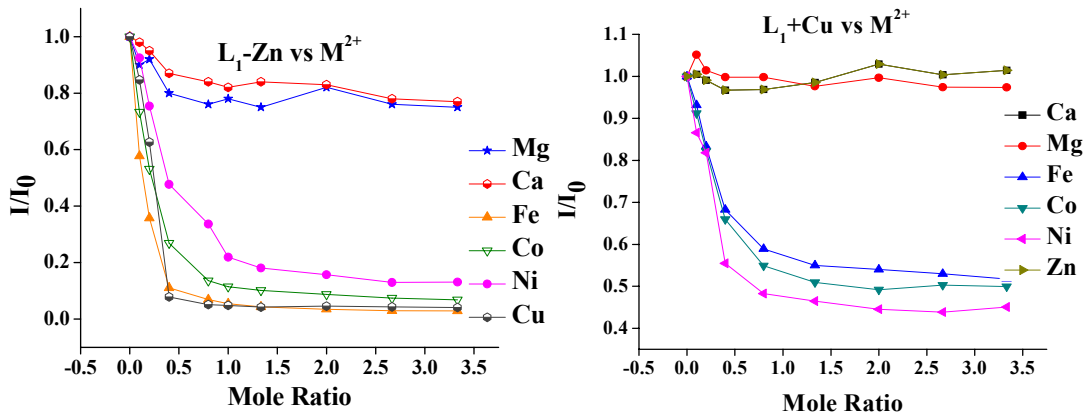

Figure F 05a. Competitive titration in methanol using L_1. (a) (RNI + 1.0 eq Zn^{2+}) vs. M^{2+} and (b) (RNI + 0.5 eq Cu^{2+}) vs. M^{2+}.

SI 06: Fluorescence spectral traces for L_3 in methanol and HEPES buffer

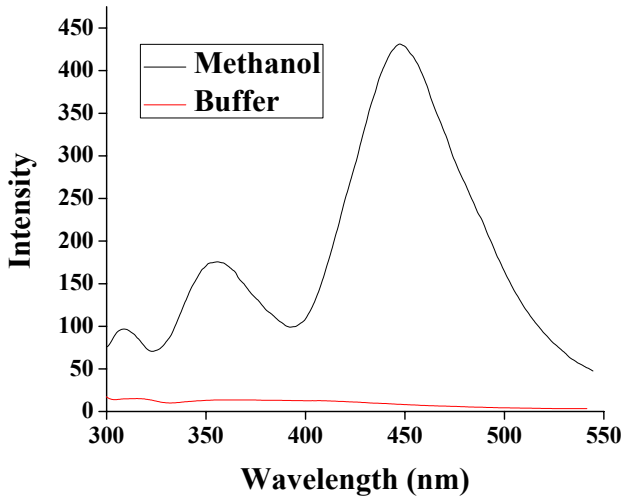

Figure F 06a. Fluorescence intensity vs. wavelength plot for L_3 in methanol and HEPES buffer (pH = 7.2) showing the decrease in intensity upon changing the solvent.

SI 07: Fluorescence titration in HEPES buffer for L_3 against M^{2+}

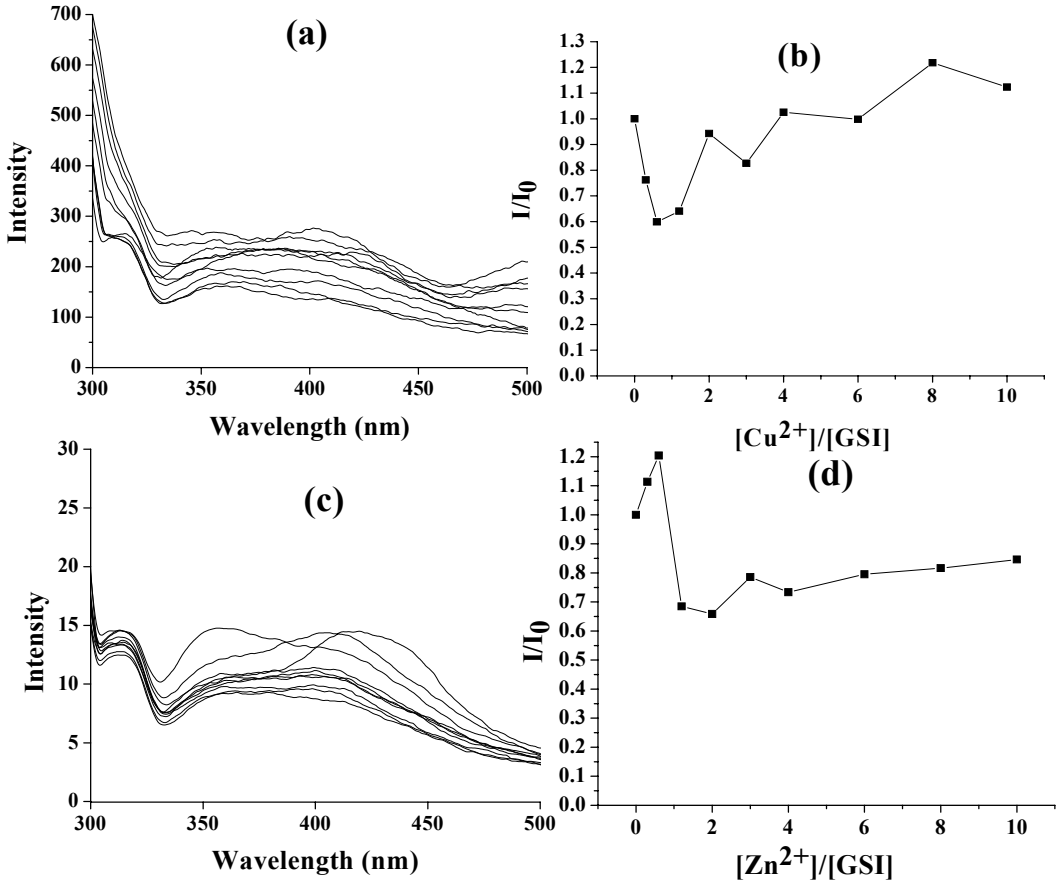

Figure F 07a. Fluorescence titration of GSI against Cu^{2+} and Zn^{2+} in HEPES buffer (pH = 7.0) showing no response at all to those two metal ions; (a) Intensity vs. Wavelength trace for GSI vs. Cu^{2+}; (b) Relative fluorescence intensity (I/I0) vs. Mole Ratio plot for GSI vs. Cu^{2+}; (c) Intensity vs. Wavelength trace for GSI vs. Zn^{2+}; (d) Relative fluorescence intensity (I/I0) vs. Mole Ratio plot for GSI vs. Zn^{2+}.

SI 08: Absorption titration for L_2 against Cu^{2+} and Zn^{2+} in HEPES buffer

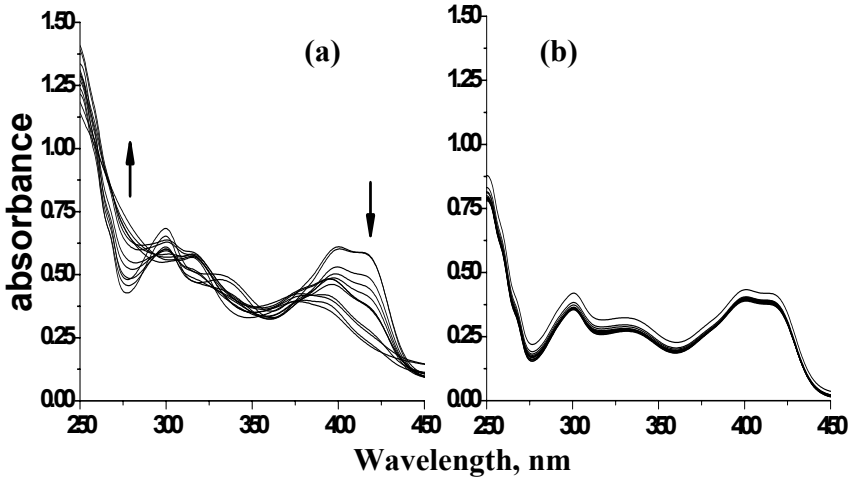

Figure F 08a. UV-Vis absorption spectra measured in the titration of M^{2+} with L_2 in HEPES buffer at different $[M^{2+}]/[L_2]$ mole ratios ranging from 0.0 to 2.0: (a) Cu^{2+}; and (b) Zn^{2+}.

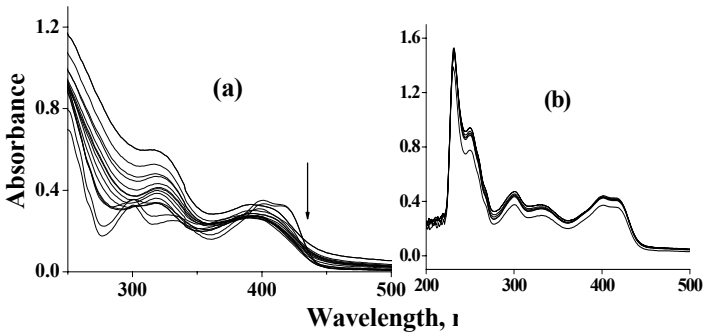

Figure F 08b. UV-Vis absorption spectra of M^{2+} titration with L_1 in HEPES buffer for (a) Cu^{2+}; (b) Zn^{2+}

SI 09: ^{1}H-NMR and mass spectral traces for the Cu(II) complexes, viz., 1, 2 and 3.

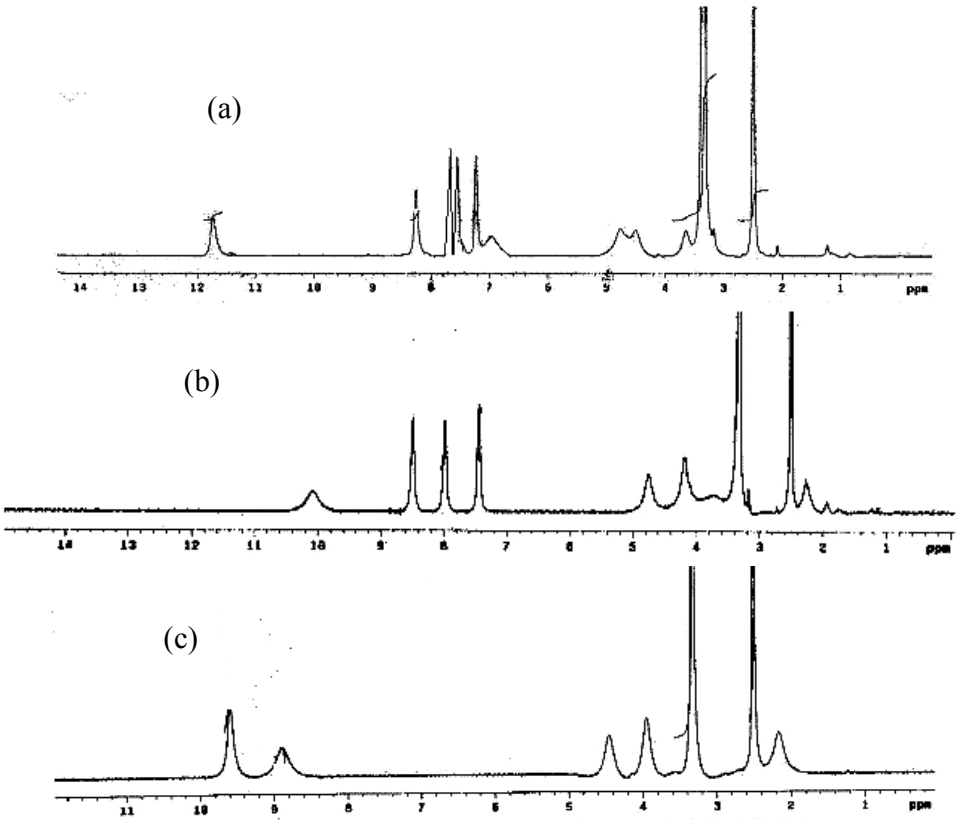

Figure F 09a. ^{1}H NMR of (a) **1**, (b) **2,** and **(c) 3**. All are recorded in DMSO-d_6.

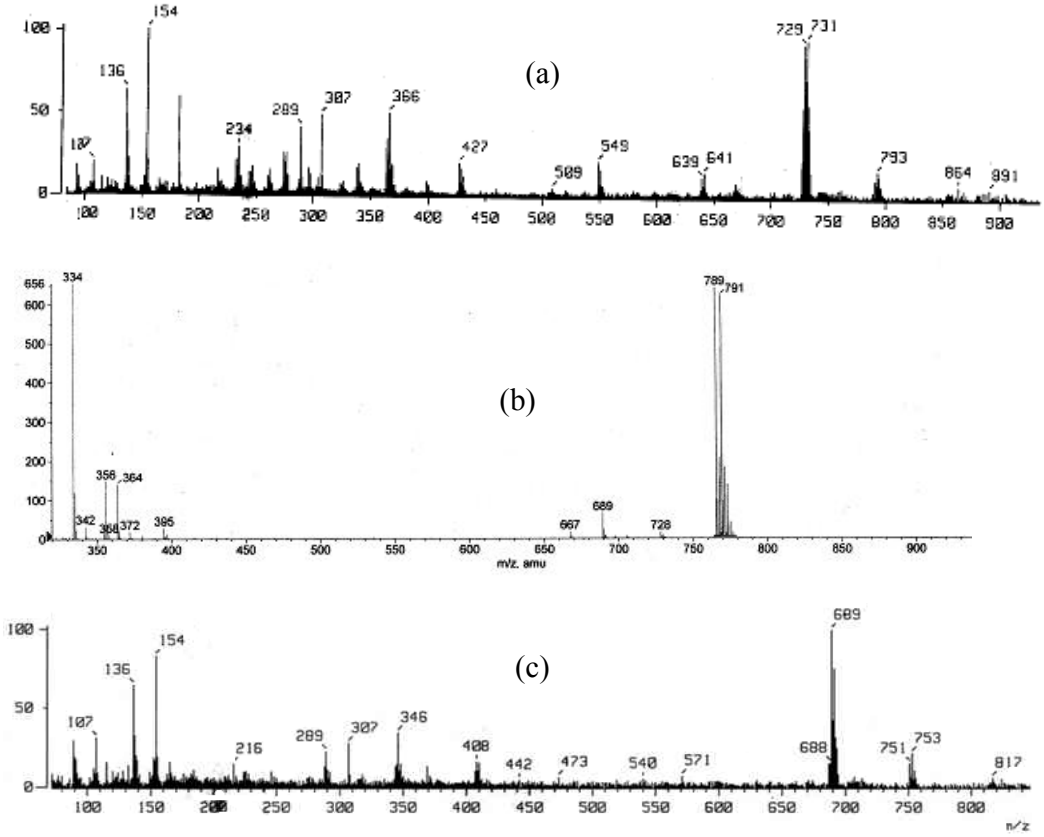

Figure F 09b. Mass spectra: (a) **1**, (b) **2** and (c) **3**.

SI 10: EPR spectral studies

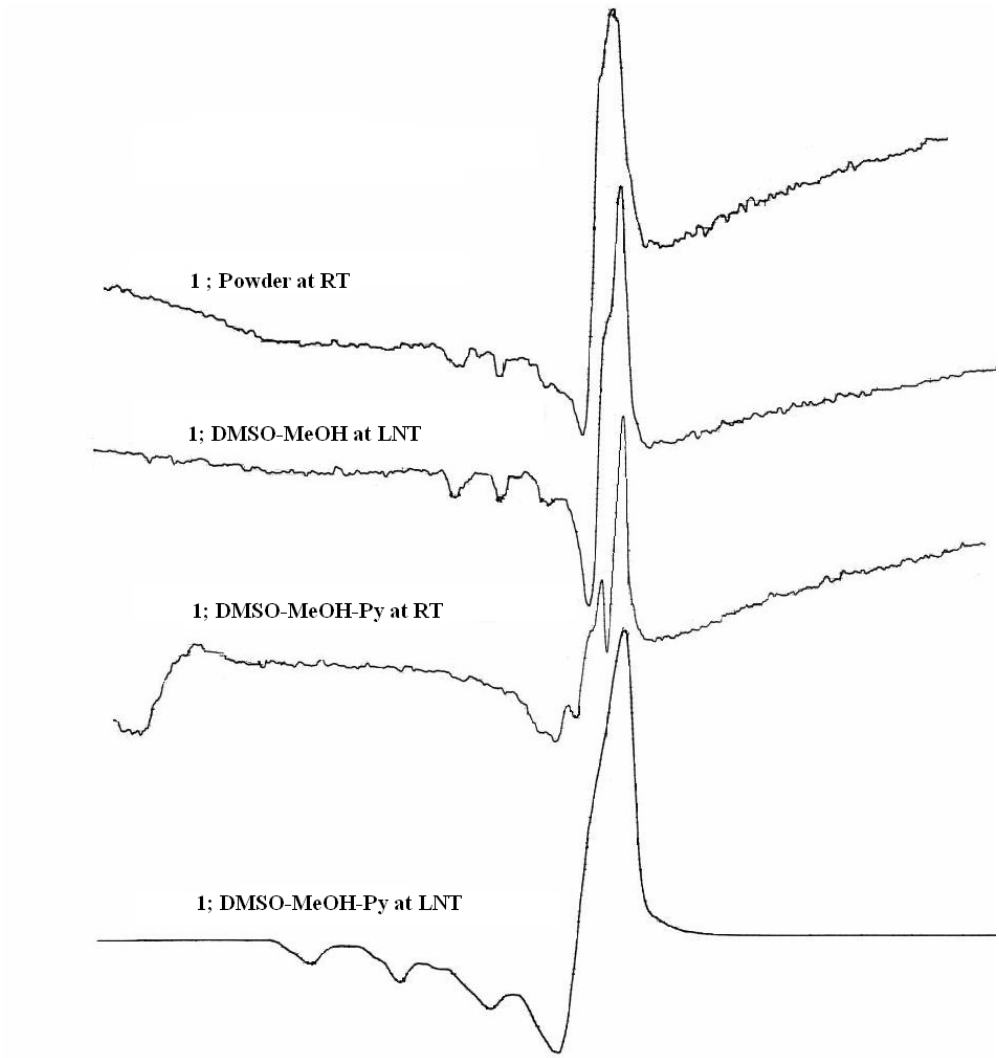

Figure F 10a. EPR spectral traces of **1** under different conditions mentioned on the spectrum. Py = pyridine; LNT = Liquid nitrogen temperature.

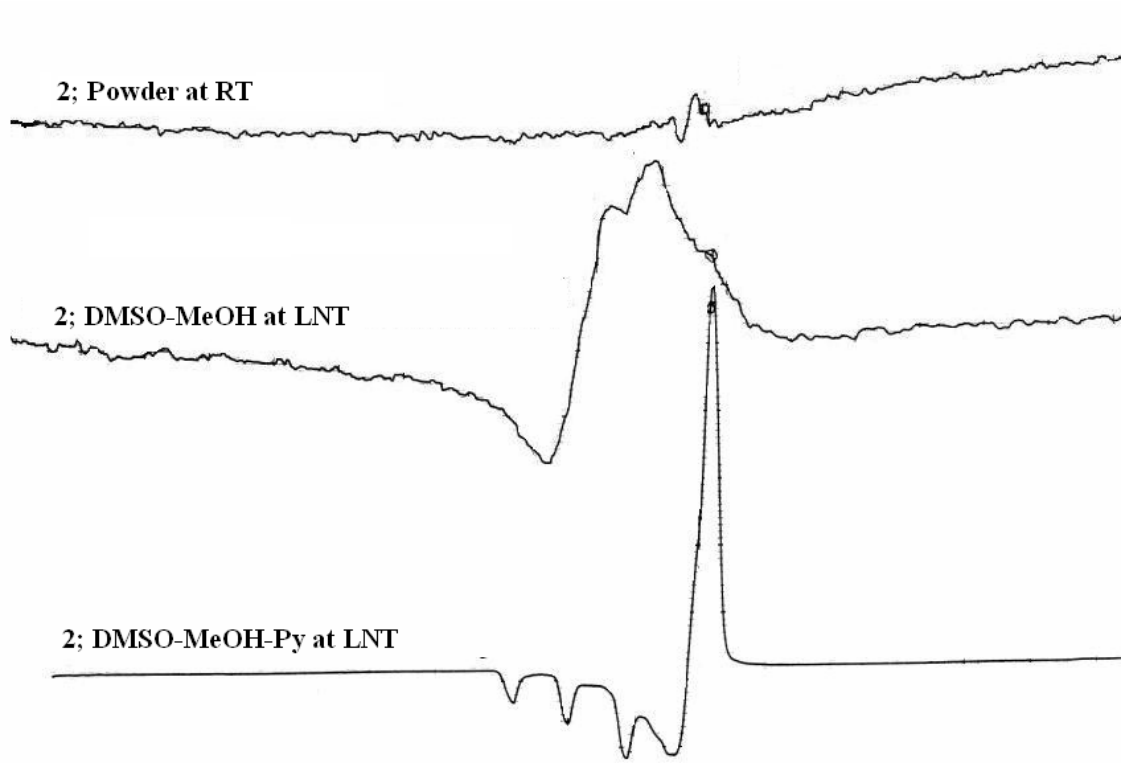

Figure F 10b. EPR spectral traces of **2** under different conditions mentioned on the spectrum. Py = pyridine; LNT = Liquid nitrogen temperature.

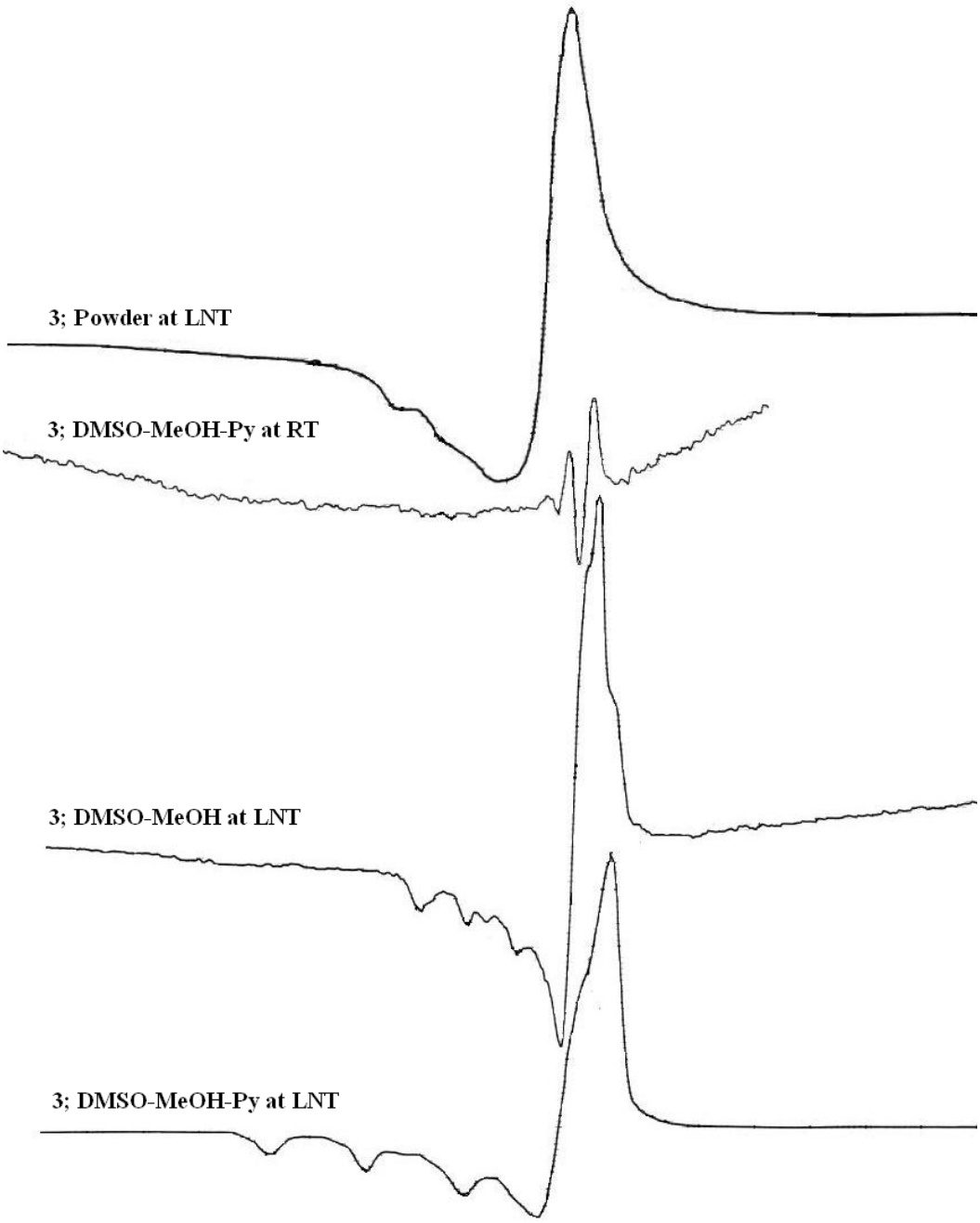

Figure F 10c. EPR spectral traces of **3** under different conditions mentioned on the spectrum. Py = pyridine; LNT = Liquid nitrogen temperature.

SI 11

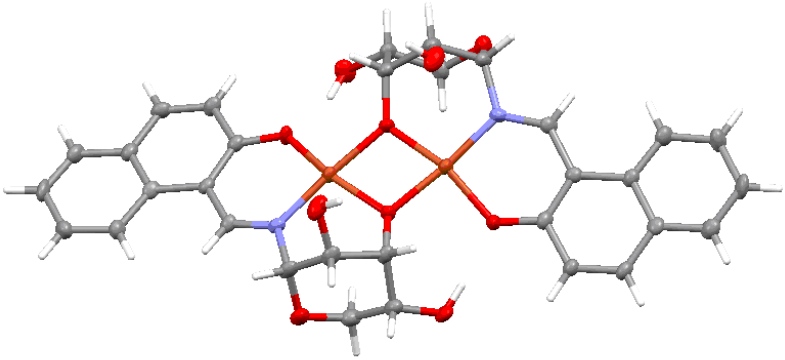

1a-(i)

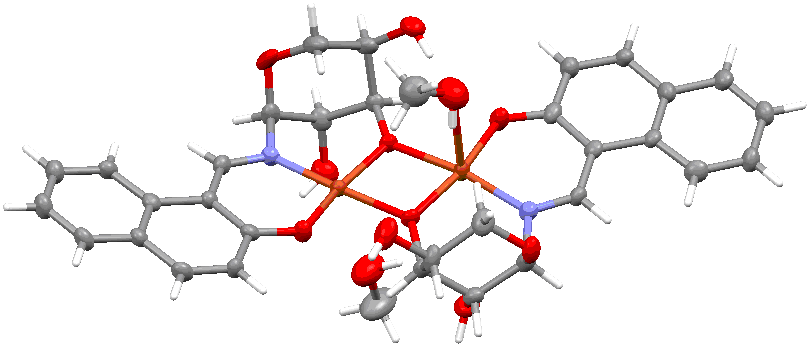

1a-(ii)

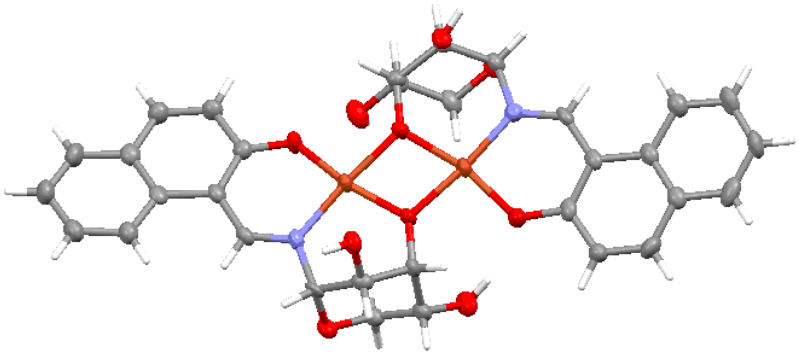

1a-(111)

Figure F 11: ORTEP view of the three dinuclear complexes 1a-(i), 1a-(ii) and 1a-(iii) in the asymmetric unit in **1a** at 150 K with thermal ellipsoids cut at the 50% probability level for non-H atoms. The dimer 1a-(i) is bounded to solvent while two others are not.

SI 12. H-bond data for the structures **1a**, **1b** and **3**

D-H—[Å]	$d_{H...A}$ (Å)	$d_{D...A}$ (Å)	<DHA(°)	Symmetry
1 a				
O31—H31O .. O34	2.013	2.840	168.0	-x+2,y+1/2,-z+1
O34—H34 .. O41	1.900	2.654	148.0	x,y,z
O40—H40 .. O30	2.150	2.835	139.0	x,y,z
O41—H41 .. O30	2.496	3.269	154.0	x,y,z
O32—H32 .. O6	1.941	2.762	166.0	x,y,z
O16--H16O .. O27	1.910	2.719	161.0	x,y,z
O20--H20O .. O16	2.010	2.816	162.0	-x+1,y-1/2,-z
O22 -- H22O .. O9	1.810	2.641	173.0	x,y,z
O26--H26O .. O33	2.040	2.858	164.0	-x+1,y-1/2,-z
O27--H27O .. O12	1.860	2.671	163.0	x,y,z
O33—H33O .. O22	1.900	2.721	165.0	x,y+1,z
1 b				
O2 -- H2O .. O6	1.960	2.791	171.0	x,y,z
O2 -- H2O .. O7	2.030	2.757	144.0	x,y,z
O3 -- H3O .. O4	1.860	2.698	172.0	-x+2,+y,-z+1
O7 -- H6 .. O5	2.700	3.438	142.7	-x+2,+y,-z+1
O6 -- H6 .. O6	2.664	3.366	142.0	-x+2,+y,-z+1
O6 -- H6 .. O7	1.986	2.710	144.0	-x+2,+y,-z+1
3				
O9—H9------O1	1.852	2.668	173.3	x,y,z
O3—H3------O7	1.911	2.692	158.8	x,y,z
O4—H4------O111	2.144	2.860	145.9	x,y,z
C18—H18-----O111	2.676	3.601	173.2	-x+1,+y+1/2,z+1
O11—H11------O4	1.925	2.733	167.3	-x+1,y+1/2,-z+1
C7—H7-----O111	2.638	3.548	165.5	-x+1,y+1/2,-z+2
O5—H5------O111	2.213	2.970	152.1	-x+1,y+1/2,-z+2